

# Detection of copiapite in the northern Mawrth Vallis region of Mars: Evidence of acid sulfate alteration



William H. Farrand<sup>a,\*</sup>, Timothy D. Glotch<sup>b</sup>, Briony Horgan<sup>c</sup>

<sup>a</sup> Space Science Institute, 4750 Walnut Street, Suite 205, Boulder, CO 80301, United States

<sup>b</sup> Department of Geosciences, Stony Brook University, Stony Brook, NY 11794, United States

<sup>c</sup> Department of Earth, Atmospheric, and Planetary Sciences, Purdue University, W. Lafayette, IN 47907, United States

## ARTICLE INFO

### Article history:

Received 14 October 2013

Revised 27 June 2014

Accepted 1 July 2014

Available online 18 July 2014

### Keywords:

Geological processes

Mars, surface

Mineralogy

Spectroscopy

## ABSTRACT

The Mawrth Vallis region on Mars is associated with extensive layered deposits containing a stratigraphic sequence of Fe/Mg smectites overlain by Al phyllosilicates. Earlier studies have reported restricted exposures of the ferric sulfate mineral jarosite on top of the sequence. In this paper we have used CRISM data covering the northern portion of the Mawrth Vallis region to find a new jarosite exposure and multiple occurrences of the mixed valence Fe-sulfate mineral copiapite ( $\text{Fe}^{2+}\text{Fe}^{3+}(\text{SO}_4)_6(\text{OH})_2 \cdot 20(\text{H}_2\text{O})$ ). HiRISE imagery indicate that the copiapite exposures lie on top of the Al phyllosilicates and thus post-date that unit either as a coating or as extensive veins. The presumed copiapite exposures are associated with high values of a "SINDX" parameter derived from CRISM data. Application of several spectral matching metrics over a spectral subsection indicated several candidates for the high SINDX phase including copiapite, ferricopiapite and metavoltine (another mixed valence Fe-sulfate mineral). Visible and near infrared CRISM spectra of the high SINDX areas are most consistent with the phase being copiapite. On Earth copiapite generally occurs as efflorescent coatings in acid mine drainage environments or in association with acid sulfate soils. The presence of jarosite and copiapite indicates the presence of acidic waters. Such acid waters could have contributed to the formation of the underlying Al phyllosilicate minerals. A possible mode of origin for these minerals in this region would involve a fluctuating ground water table and the weathering of Fe sulfide minerals.

© 2014 Elsevier Inc. All rights reserved.

## 1. Introduction

The Mawrth Vallis region on Mars (Fig. 1), located between 18–28°N and 337–350°E, has been a focus of interest for Mars researchers since it was recognized from orbital OMEGA hyperspectral imagery as the largest exposure of phyllosilicate minerals on the planet (Bibring et al., 2005). Numerous studies of the region have revealed a basic stratigraphy of a basal layer, of over 100 m thickness, of Fe/Mg smectite-bearing layered rocks overlain by a unit of approximately 10–50 m thickness, containing Al-bearing phyllosilicates and hydrated silica (Bishop et al., 2008; Loizeau et al., 2010; Noe Dobrea et al., 2010, 2011). Original interpretations of the origins of phyllosilicates present at Mawrth Vallis, and associated environmental implications, concentrated on the fact that smectite clays, such as those in the Fe/Mg smectite bearing unit, would most likely originate in a neutral to alkaline aqueous environment (Bibring et al., 2006). Such an environmental scenario

stands in contrast to the environmental conditions suggested by the presence of massive sulfate deposits in the early Hesperian-aged terrains of Terra Meridiani, Valles Marineris and elsewhere (Bibring et al., 2005; Gendrin et al., 2005; Murchie et al., 2009) and the identification of jarosite in the Burns Formation of Meridiani Planum by the Opportunity rover (Squyres et al., 2004; Klingelhöfer et al., 2004; McLennan et al., 2005). Thus, the older, phyllosilicate-rich terrains at Mawrth Vallis and elsewhere on the planet have been used to infer that wet and neutral aqueous environments were more common on early Mars (e.g. Bibring et al., 2006).

The known mineralogy of the Mawrth Vallis region became more diverse with the discovery of bassanite, a calcium sulfate formed in neutral pH conditions, nominally situated near the base of the sequence (Wray et al., 2010). Also, the discovery of a seemingly isolated exposure of jarosite, located near the top of the stratigraphic sequence (Farrand et al., 2009) indicated more acidic aqueous mineral formation conditions. Additionally, Noe Dobrea et al. (2011) observed scattered occurrences across the region of a spectral signature similar to that of an "acid leaching product"

\* Corresponding author.

E-mail address: [farrand@spacescience.org](mailto:farrand@spacescience.org) (W.H. Farrand).

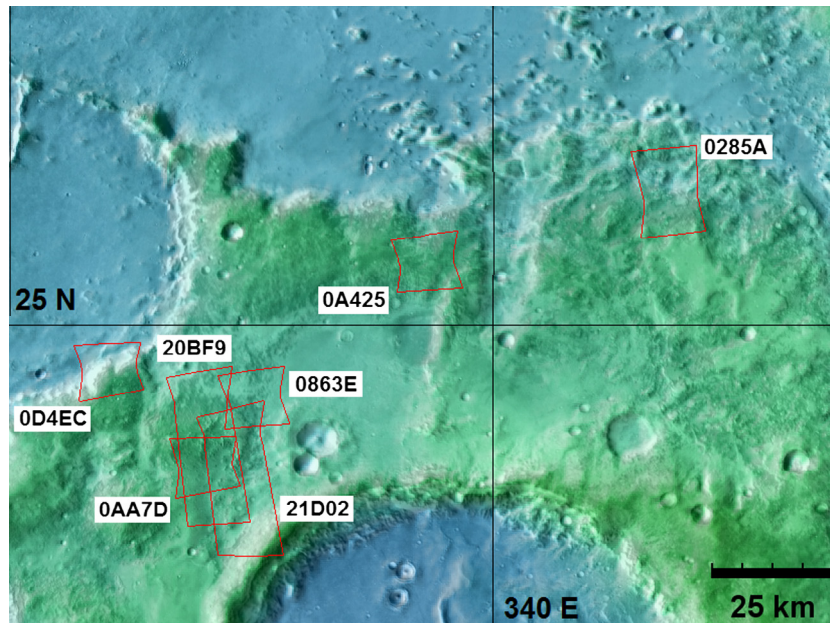


**Fig. 1.** Colorized MOLA elevation overlain on THEMIS mosaic of the northern Mawrth Vallis region. CRISM stamps of the scenes referenced in the text are overlaid in red. (For interpretation of the references to color in this figure legend, the reader is referred to the web version of this article.)

observed by Roach et al. (2010) in Valles Marineris deposits and also some scattered exposures of spectra again consistent with jarosite. Michalski et al. (2013) also noted another occurrence of jarosite similar to that described by Farrand et al. (2009).

The emerging picture is one in which acidic conditions played a role in the formation of at least the upper “Al phyllosilicate” unit in the Mawrth Vallis stratigraphy. It has been suggested that a likely formation scenario would be one similar to the pedogenesis of Al-clay bearing soils in some terrestrial locations (Horgan et al., 2013). Kaolinite, or one of several kaolinite group minerals (e.g., kaolinite, dickite, nacrite or halloysite), has been recognized as occurring near the top of the Al phyllosilicate unit. Kaolinite group minerals have also been recognized amongst Al phyllosilicates associated with other similar exposures of “stratigraphy” (Ehlmann et al., 2011) or “plateau” phyllosilicates (Le Deit et al., 2012). Kaolinite group minerals can be associated with acid leaching (Gaudin et al., 2011). The effect of weathering through acidic solutions also results in the formation of a number of sulfate minerals (e.g., Tosca et al., 2004). However, while sulfate minerals associated with acidic conditions have been observed in restricted occurrences in the Mawrth Vallis region, their presence has not been recognized as widespread across the region.

We report here on observations of a number of occurrences of ferric and mixed valence Fe-sulfate minerals across the northern portion of the Mawrth Vallis region shown in Fig. 1. We have utilized spectral parameter maps derived from CRISM data to screen for possible occurrences of sulfate minerals. Having identified areas that could have exposures of these minerals, we have extracted average region of interest (ROI) spectra for these areas and examined ratio spectra of those ROI average spectra. We have also examined visible and near infrared (VNIR) spectra from CRISM’s “S” detector, and merged CRISM VNIR and short-wave infrared (SWIR) “L” detector data to provide additional information on the identity of the putative sulfate minerals.

## 2. Sulfate mineral reflectance features

Cloutis et al. (2006) performed a detailed study of the reflectance spectra of 42 sulfate minerals. Over the reflected solar wavelength range, spectral features in sulfate minerals are caused

by the presence of OH, H<sub>2</sub>O, or metal cations bonded to anions in the mineral structure. Specific absorption features differing from those commonly occurring in other hydrated minerals include absorption features in the 1.75–1.78 μm range, and in the 2.4–2.55 μm range (Fig. 2). The former feature is attributable to OH and/or H<sub>2</sub>O vibrational overtones and/or to bonds between these molecules and constituent cations (Cloutis et al., 2006). Sulfates can exhibit multiple features in the 2.4–2.55 μm range, caused by the 3ν<sub>3</sub> S–O overtone, the ν<sub>OH/H<sub>2</sub>O</sub> + γ/δ<sub>OH/H<sub>2</sub>O</sub> overtone, or some combination of 3ν<sub>3</sub> S–O or OH/H<sub>2</sub>O combinations and/or overtones (Cloutis et al., 2006). We searched for spectral features in the 2.4–2.55 μm range in the CRISM scenes examined as potential evidence for the presence of sulfate minerals.

Cloutis et al. (2006) also noted that absorption features attributable to Fe<sup>2+</sup> occurred near 0.92–0.947 μm in rozenite and melanterite with both also having a secondary Fe<sup>2+</sup> absorption near 1.17 μm and that copiapite has those features near 0.9 and 1.17 μm. Copiapite also has a Fe<sup>3+</sup> band caused by the <sup>6</sup>A<sub>1g</sub> → <sup>4</sup>T<sub>1g</sub> transition centered near 0.855–0.866 μm and jarosite has that band centered near 0.933 μm. Copiapite and jarosite also have sharp absorption bands caused by the <sup>6</sup>A<sub>1g</sub> → (<sup>4</sup>A<sub>1g</sub>, <sup>4</sup>E<sub>g</sub>) transition centered at 0.430 and 0.435 μm respectively.

## 3. Data and data reduction

As one of the “final four” candidate areas for the landing site of the Mars Science Laboratory rover Curiosity, and as a leading candidate for potential future landed science missions, a significant number of CRISM Half Resolution Long (HRL) and Full Resolution Targeted (FRT) scenes and HiRISE images have been collected over the Mawrth Vallis region. The CRISM instrument is described more fully in Murchie et al. (2007) but, briefly, it utilizes two spectrometers, an “S” detector covering the wavelength region from 0.36 to 1.05 μm, and an “L” detector covering the wavelength region from 1.0 to 3.9 μm.

CRISM “L” detector data were converted, using the CRISM Analysis Tools (CAT) add-on module to the commercial ENVI software (Exelis Visual Information Systems, 2012), to apparent surface reflectance using a “volcano scan” atmospheric correction approach (Langevin et al., 2005). Regions of interest (ROIs) with spectral

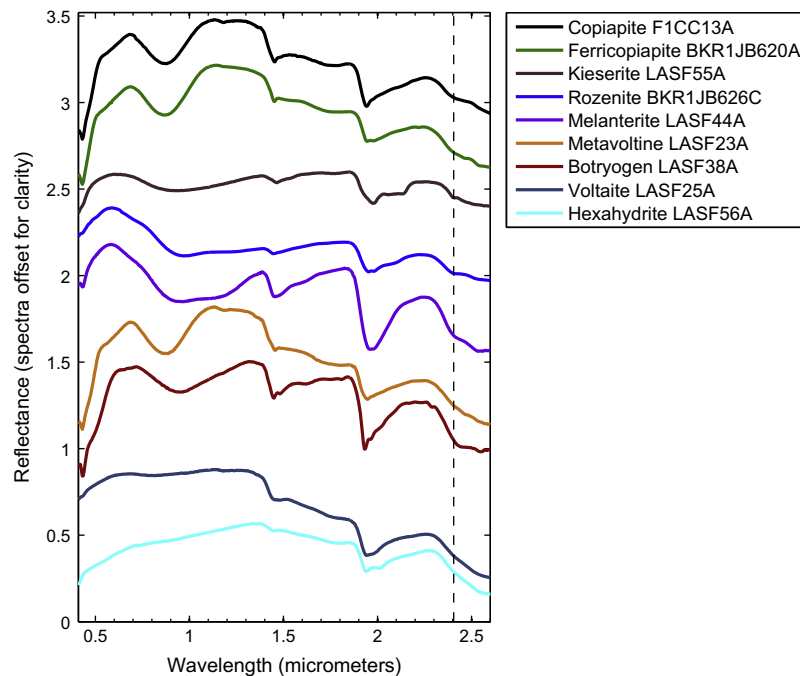


**Fig. 2.** Reflectance spectra of select Fe and Mg bearing sulfates. The bend, or in some cases more clearly defined band, in the 2.4  $\mu\text{m}$  region is marked by a dashed line.

features indicative of sulfate minerals were identified in the volcano scan corrected data as will be described below. Data were smoothed using the CIRRUS data denoising approach (Parente, 2008) resident in the CAT software. Where spectrally flat areas lay within the same range of columns of the scene, ROI pixels from within a column were averaged together and then divided by an average of pixel spectra from a spectrally neutral region within the same column. Then, the ratio spectra from a set of columns were averaged together. Generally, the ROI spectra consisted of 9–12 pixel spectra.

CRISM “S” detector data (covering the 0.41–1.02  $\mu\text{m}$  VNIR range) were also utilized. CRISM data from the PDS are available in the form of exo-atmospheric radiance factor. This data is affected by atmospheric dust with the consequence that “S” detector data, without any correction, look very similar across a scene. All the “S” detector spectra show a UV–Vis absorption edge so there are no “truly flat” spectra to use as a denominator. However, spectra with that UV–Vis absorption edge but lacking other absorptions served as effective denominator spectra. When corresponding sets of pixels from the “S” and “L” detectors were ratioed by approximately the same spectrally “flat” areas, they could be merged for combined range ratio spectra.

## 4. Methodology

### 4.1. Use of spectral parameters for survey

In order to screen for portions of CRISM FRT or HRL scenes that might contain sulfate minerals, we examined “SINDEX” parameter images in the on-line catalog of parameter images derived from CRISM scenes that is hosted by Arizona State University (<http://viewer.mars.asu.edu/planetview/>). The SINDEX parameter (Pelkey et al., 2007; Flahaut, 2011) is a measure of the convexity of spectra at 2.29  $\mu\text{m}$  which can result from water and/or sulfate molecule absorptions in the 1.9–2.1  $\mu\text{m}$  region and/or at 2.4  $\mu\text{m}$ . It is defined as:

$$\text{SINDEX} = 1 - (\text{R2100} + \text{R2400}) / (2 * \text{R2290}) \quad (1)$$

where R2100 is the reflectance at 2100 nm, R2400 is the reflectance at 2400 nm and R2290 is the reflectance at 2290 nm. Surfaces

hosting sulfate minerals with these absorption bands will display a higher level of convexity (i.e. a “sharper bend”) at 2.29  $\mu\text{m}$ . Sulfate minerals that have an absorption near 2.29  $\mu\text{m}$ , such as jarosite with its 2.265  $\mu\text{m}$  band, will not return a high SINDEX value and so other parameters or search methods must be used to detect them. A number of scenes, listed in Table 1, with coherent regions displaying high values of the SINDEX parameter in the on-line catalog of images were downloaded and atmospherically corrected as described above. Pixel spectra were interactively examined over such high SINDEX areas. ROIs were defined that included those spectra showing absorption features attributed to sulfate minerals as described in Section 2.

Another method that we have used to specifically detect occurrences of jarosite, or jarosite-like, spectral signatures (e.g., the doublet associated with the “acid leaching products” described by Roach et al. (2010)) is the “Doub2200” parameter (Roach et al., 2010; Noe Dobrea et al., 2011; Flahaut, 2011). The Doub2200 parameter is defined as:

$$\text{Doub2200} = 1 - ((\text{R2205} + \text{R2258}) / (\text{R2172} + \text{R2311})) \quad (2)$$

where R2205 is the reflectance at 2205 nm, R2258 is the reflectance at 2258 nm, and so on.

Doub2200 parameter images are not available on the ASU image catalog referenced above, so this parameter was calculated using the CRISM CAT software package for ENVI for the scenes listed in Table 1 that had been identified and downloaded on the basis of observed high SINDEX values. Regions with high Doub2200 values were compared to 2.5, 1.5, and 1.08  $\mu\text{m}$  (RGB) composite images to see if they corresponded with the unique color unit described in the following section. Spectra from these regions were also examined to look for the distinctive 2.265  $\mu\text{m}$  band associated with jarosite (Bishop and Murad, 2005).

### 4.2. Color composites

Jarosite-bearing exposures, such as those observed by Farrand et al. (2009) and Michalski et al. (2013) in northern Mawrth Vallis have a distinctive color in a color composite of the 2.5, 1.5, and 1.08  $\mu\text{m}$  CRISM bands. With reference to Munsell color charts,

**Table 1**  
Scenes analyzed with Lat./Lon. positions of examined high SINDX and/or Doub220 exposures.

Scene	High SINDX	High Doub2200
FRT0000863E	24.69°N, 338.97°E	–
HRL000043EC	24.69°N, 339.01°E, 24.68°N, 339.03°E	–
FRT0000D4EC	24.76°N, 338.62°E	–
FRT0000AA7D	24.56°N, 338.78°E, 24.55°N, 338.92°E	–
FRT00020BF9	24.67°N, 338.78°E	24.72°N, 338.77°E; 24.78°N, 338.76°E
FRT0000A425	25.31°N, 339.77°E	25.32°N, 339.75°E

the color of the jarosite bearing unit in these scenes in this particular composite of bands is moderate orange pink to pale yellowish orange in color. This color unit is illustrated in Fig. 3 with the jarosite exposures noted in the previous two paper citations and new areas found in this study.

#### 4.3. Spectral matching metrics

In order to determine if the spectral features noted in the ROI average spectra can indeed be attributed to sulfate minerals, and what those minerals might be, a set of spectral matching techniques was used on subsections of these ROI spectra. The spectral matching metrics that were used were a spectral feature fitting (SFF) approach (Clark et al., 1990), a spectral similarity value (SSV) metric utilizing a dimensionally adjusted Euclidean distance measure and a directional correlation metric (Granahan, 2002), and a Pearsonian correlation coefficient (PCC) metric (Abilio de Carvalho and Meneses, 2000). These spectral matching approaches are described briefly below.

##### 4.3.1. Spectral feature fitting

The spectral feature fitting (SFF) approach consists of a comparison of a continuum-removed absorption band measured by a field, air- or spaceborne spectrometer to a collection of laboratory measured spectral library spectra with a roughly similar absorption feature in order to determine the best match in terms of spectral shape and position. The continuum removal is achieved by the selection of bands defining the shoulders of the absorption band, calculation of a straight line between the shoulders, and then division of the measured reflectance values by the calculated straight line continuum values (Clark and Roush, 1984). As described by Clark et al. (1990), the SFF procedure then takes the continuum-removed observed and measured spectra, adjusts the contrast of the features, and then performs a linear least squares fit between the two. The  $R^2$  coefficient (Woolridge, 2012) is the goodness of fit metric used to compare the library and measured spectra. Identical spectra would have a  $R^2$  value of 1.

##### 4.3.2. Spectral similarity value

Granahan (2002) described a combined spectral similarity value (SSV) metric that utilizes a dimensionally adjusted Euclidean distance (DAED) metric that is sensitive to the difference in magnitude between two spectra and a directional correlation (DC) metric that is sensitive to spectral shape, but is not affected by overall albedo differences between two spectra. More detail on these metrics are provided in Granahan (2002). The combined SSV is defined here as:

$$SSV = 1 - \sqrt{DAED^2 + DC^2} \quad (3)$$

Granahan (2002) defined the SSV as just the quantity under the radical; however, here, for better comparison with the other metrics, SSV is defined as being 1 minus the combined DAED and DC values

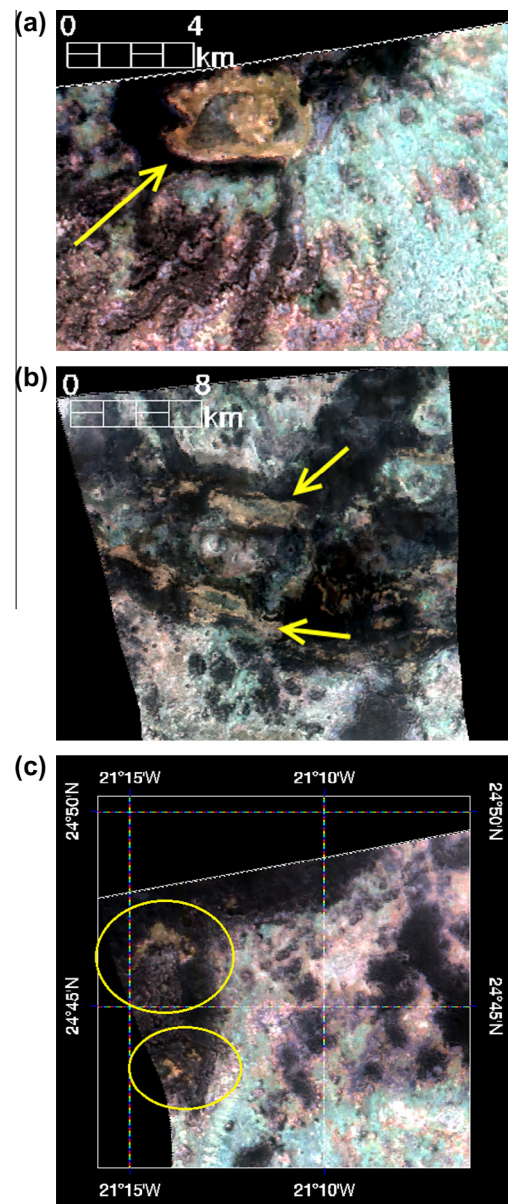


**Fig. 3.** (a) Composite of 2.5, 1.5 and 1.08  $\mu\text{m}$  bands of subsection of the CRISM scene FRT0000A425 with jarosite-bearing area (Farrand et al., 2009) and unique color unit indicated by arrow. Jarosite-bearing region is centered at  $\sim 25.33^\circ\text{N}$ ,  $20.25^\circ\text{W}$ . (b) Subsection of composite of 2.5, 1.5 and 1.08  $\mu\text{m}$  bands of the CRISM scene HRL0000285A with jarosite-bearing areas (Michalski et al., 2013) and associated unique color unit indicated by arrows. Center of subsection is at  $\sim 25.58^\circ\text{N}$ ,  $19.32^\circ\text{W}$ . (c) Subsection of CRISM scene FRT00020BF9 with areas circled with jarosite signatures. (For interpretation of the references to color in this figure legend, the reader is referred to the web version of this article.)

so that like the SFF metric of two identical spectra would have an SSV of 1.

#### 4.3.3. Pearsonian correlation coefficient

Abilio de Carvalho and Meneses (2000) described a spectral correlation coefficient that incorporated the Pearsonian correlation coefficient. This metric is defined as:

$$PCC = \frac{\sum_{i=1}^n (X_i - \bar{X})(Y_i - \bar{Y})}{\sqrt{\sum_{i=1}^n (X_i - \bar{X})^2} \sqrt{\sum_{i=1}^n (Y_i - \bar{Y})^2}} \quad (4)$$

where PCC is the Pearsonian correlation coefficient,  $X_i$  is the  $i$ th band of target spectrum  $X$ ,  $\bar{X}$  is the mean of spectrum  $X$ ,  $Y_i$  is the  $i$ th band of library spectrum  $Y$ ,  $\bar{Y}$  is the mean of library spectrum  $Y$ , and  $n$  is the number of bands. As with the previous two metrics, identical spectra would have PCC values of 1.

## 5. Application of methodology

### 5.1. ROI selection

Spectra were interactively examined over the high SINDX areas of the scenes listed in Table 1. Special attention was paid to the 2.29–2.6  $\mu\text{m}$  region since, as noted in Section 2, this is a region where sulfate minerals can display a diagnostic absorption feature or features. An asymmetric absorption band with a minimum at approximately 2.4  $\mu\text{m}$ , often occurring with a second band centered at approximately 2.52  $\mu\text{m}$  was observed in the volcano scan corrected and denoised versions of some scenes and subsequently sought in others. We also note that these are weak spectral features. To be fully recognized, continuum-removed spectra needed to be examined. Regions of interest (ROIs) were defined for areas displaying absorption features centered near 2.4 and 2.52  $\mu\text{m}$ . Representative CIRRUS-denoised spectra from the FRT0000AA7D and FRT0000863E scenes are shown in Fig. 4. In the full SWIR range spectra of Fig. 4A, a 2.2  $\mu\text{m}$  band is present, indicating that the high SINDX materials occur in the Al phyllosilicate unit. Weak absorption bands near 2.4 and 2.52  $\mu\text{m}$  are present that are more apparent in the continuum-removed spectra of Fig. 4C. These features are interpreted as evidence of the presence of sulfate-bearing materials on top of, or conceivably mixed in with the Al phyllosilicate unit.

The Doub2200 parameter image also was calculated for the scenes listed in Table 1. For regions with high Doub2200 values, the 2.5, 1.5, and 1.08  $\mu\text{m}$  color composite was also examined to see if the color unit described above was present over the high Doub2200 areas. The combination of both the high Doub2200 values and the color unit was only observed (besides in the already-recognized FRT0000A425 (Farrand et al., 2009) and HRL0000285A

(Michalski et al., 2013) scenes) in the FRT00020BF9 scene. The HRL0000285A was not considered further due to what was deemed a poor volcano scan atmospheric correction and the fact that it was discussed more extensively by Michalski et al. (2013). In the high Doub2200 areas, ROIs were formed from pixels with an absorption feature centered at, or near 2.265  $\mu\text{m}$ .

### 5.2. Examination of ratio spectra

To gain additional detail on the spectra with features in the 2.29–2.6  $\mu\text{m}$  region, ratio spectra were calculated based on the procedure described above of dividing an average of target pixels from within a column by an average of spectrally neutral pixels from within the same column and then averaging the column ratios from several columns together. The ratio spectra are shown in Fig. 5. In some of the spectra the asymmetric band near 2.4  $\mu\text{m}$  resolves into a doublet with a shoulder to weak band at 2.45  $\mu\text{m}$  so that the whole assemblage of bands centered near 2.4, 2.45, and 2.52  $\mu\text{m}$  can appear as a triple absorption.

For the unique color unit in the FRT00020BF9 scene, a representative ratio spectrum of pixels showing the 2.265  $\mu\text{m}$  feature characteristic of jarosite is shown in Fig. 6a. Comparison of the 2.265  $\mu\text{m}$  feature to a K-jarosite lab spectrum in Fig. 6b shows the match of the CRISM spectrum to a laboratory jarosite.

### 5.3. Spectral matching of ROI average spectra

The high SINDX areas are generally coincident with areas that were high in the BD2200 parameter (i.e., having a strong absorption band centered at approximately 2.2  $\mu\text{m}$ ); thus the sulfate mineral or minerals occurring in these pixels are present in combination with other minerals, including the Al-phyllosilicates that cause strong 2.2  $\mu\text{m}$  bands (Figs. 4a and 5a) throughout the region. Such mixed pixel spectra typically frustrate spectral matching approaches when the full spectral range is used. However, by utilizing the spectral subsection over the 2.29–2.6  $\mu\text{m}$  range, a region in which sulfate minerals can have absorption features that are potentially more diagnostic, a better comparison to possible sulfate mineral spectra was achievable. The spectral matching metrics described above were applied to the 2.29–2.6  $\mu\text{m}$  subsection of CRISM ROI average ratio spectra displaying absorption features in this spectral range. Spectral matching was performed using continuum-removed versions of the ratio spectra from Fig. 5 (along with several other high SINDX ROI ratio spectra) and compared against continuum-removed library spectra over the same spectral range. The CRISM ratio spectra were matched against a set of 109

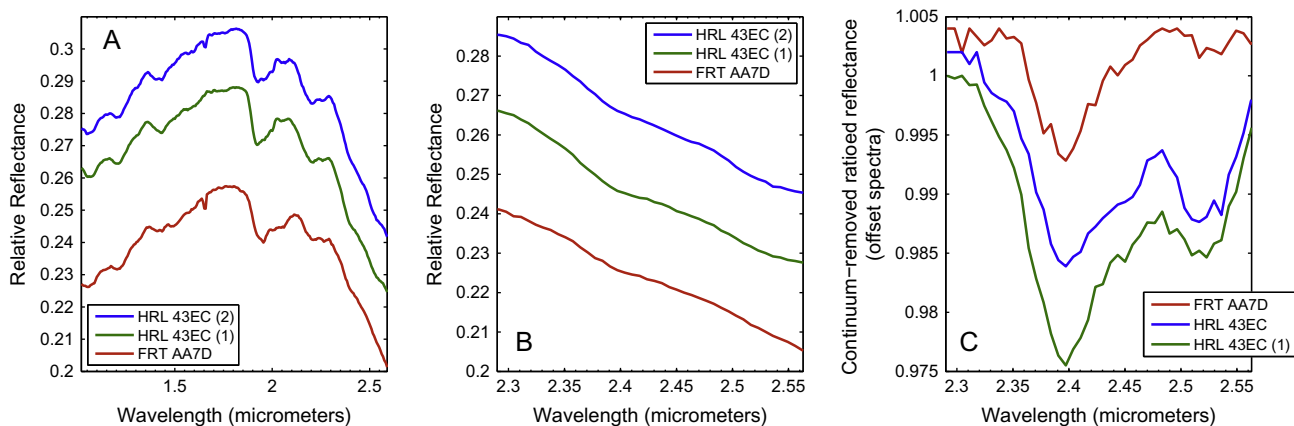
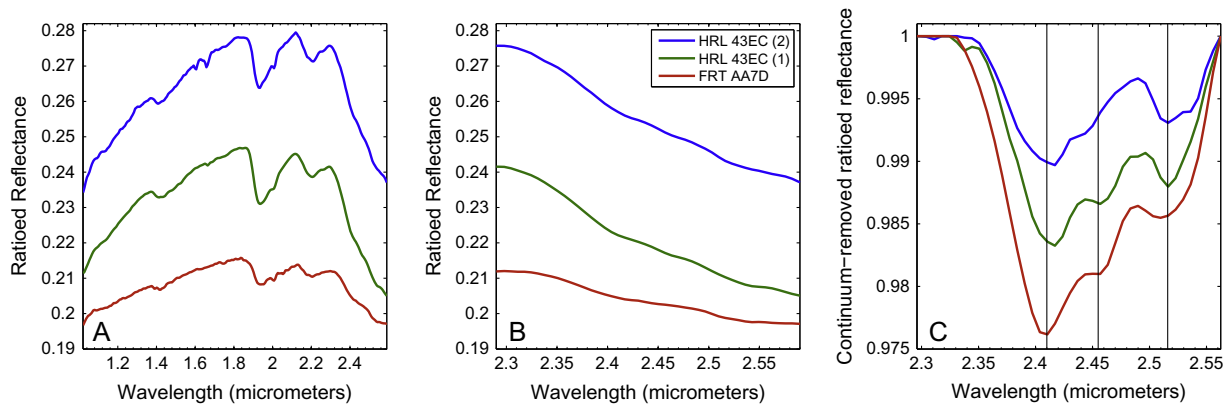
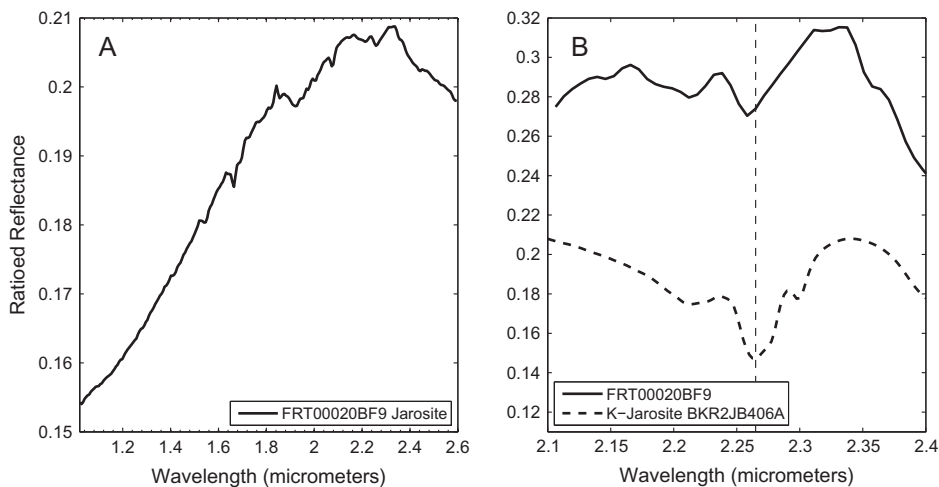


Fig. 4. (A) Full 1.05–2.56  $\mu\text{m}$  range volcano scan-corrected, CIRRUS denoised spectra of high SINDX areas in the CRISM scenes HRL 43EC and FRT AA7D. (B) 2.29–2.56  $\mu\text{m}$  spectral subsections of ROI average spectra from (A) of high SINDX areas in the CRISM scenes HRL 43EC and FRT AA7D. (C) Continuum-removed version of the spectra in (B).



**Fig. 5.** (A) Full 1.05–2.56  $\mu\text{m}$  range spectra of high SINDX areas in the CRISM scenes HRL 43EC and FRT AA7D ratioed to spectrally neutral spectra. (B) 2.29–2.56  $\mu\text{m}$  spectral subsections of ROI average spectra from (A) of high SINDX areas in the CRISM scenes HRL 43EC and FRT AA7D. (C) Continuum-removed version of the spectrum in (B) with vertical lines highlighting absorptions that are most evident in the HRL 43EC spectra.



**Fig. 6.** (A) ROI average of ratios from scene FRT00020BF9 of nominal jarosite-bearing area. (B) Focus on the 2.265  $\mu\text{m}$  band region. Dashed line is centered at 2.265  $\mu\text{m}$  band and compares the FRT00020BF9 spectrum with CRISM spectral library K-jarosite spectrum BKR2JB406A.

hydrated mineral spectra from the CRISM, USGS, and RELAB spectral libraries (Murchie et al., 2007; Clark et al., 2007; Pieters and Hiroi, 2004). These included phyllosilicates, hydrated silica, zeolites, as well as sulfates. Spectra with features (such as a band near 2.3  $\mu\text{m}$ ) that were clearly missing from the high SINDX ROI ratio spectra, were excluded from the library. Results are shown in Table 2. Since the spectral matches are tentative, the three highest scoring library spectra for each ROI average spectrum are shown. Full-range library spectra of the minerals most often chosen by the spectral matching are shown in Fig. 7a and continuum-removed versions of the spectra over the 2.29–2.6  $\mu\text{m}$  range are shown in Fig. 7b.

The observation of a distinct 2.265  $\mu\text{m}$  band was considered evidence of the presence of jarosite and so the spectral matching metrics were not applied to the 2.265  $\mu\text{m}$  band region for the jarosite detections in the FRT00020BF9 scene. Additional confirmation of jarosite in that scene was provided through analysis of VNIR range spectra from the CRISM “S” detector as discussed in the next section.

#### 5.4. Examination of “S” detector data

In order to gain additional perspective on the identity of the sulfate phase or phases that are present in association with the high SINDX areas, we also examined the CRISM “S” detector VNIR-range

data over these areas. VNIR ratio spectra from high SINDX areas from several scenes are shown in Fig. 8A. These spectra can be compared against “S” detector spectra (Fig. 8B) from jarosite-bearing areas in the FRT000A425 scene discussed in Farrand et al. (2009) and the jarosite region in FRT00020BF9 first described here. The spectra from the high SINDX areas have a continuum-removed NIR band minimum which varies somewhat between the ROI spectra extracted from the different scenes but ranges from approximately 0.86–0.9  $\mu\text{m}$ , a relative reflectance maximum at approximately 0.69  $\mu\text{m}$ , and many of the spectra from these regions have a sharp absorption centered at 0.43  $\mu\text{m}$ . Some of the variability between the different high SINDX ROI spectra could be attributable to contamination from other phases within the ROIs and/or effects from the denominator spectra. The jarosite-bearing areas have a continuum-removed NIR band minimum at approximately 0.89  $\mu\text{m}$  and a relative reflectance maximum at approximately 0.7  $\mu\text{m}$ .

## 6. Discussion of results

### 6.1. Identity of sulfate phases

Examination of CRISM “L” detector data clearly indicate the presence of jarosite in several sites in the FRT00020BF9 scene

**Table 2**  
Spectral matches over the 2.29–2.59  $\mu\text{m}$  interval using the three spectral matching approaches discussed in the text. For some scenes, more than one region of interest over a high SINDX region is given. For each ROI, the top three matches and their scores are presented for each matching metric. Descriptions of these minerals are provided in Table 3.

Scene/ROI	Mineral	SFF	Mineral	PCC	Mineral	SSV
FRT A425	Copiapite C1JB969	0.9276	Melanterite LASF44A	0.9723	Ferricopiapite BKR1JB620A	0.9220
FRT A425	Botrygen LASF38A	0.9177	Copiapite C1JB969	0.9679	Amarantite LASF26A	0.9067
FRT A425	Melanterite LASF44A	0.9027	Mg sulfate CJB366	0.9651	Copiapite BKR1LH52	0.9023
HRL 43EC/1	Kieserite LASF55A	0.9296	Melanterite LASF44A	0.9792	Kieserite LASF55A	0.9299
HRL 43EC/1	Botrygen LASF38A	0.9265	Botrygen LASF38A	0.9722	Amarantite LASF26A	0.9233
HRL 43EC/1	Copiapite C1JB969	0.8959	Kieserite LASF55A	0.9709	Metavoltine LASF23A	0.9227
HRL 43EC/2	Kieserite LASF55A	0.9446	Kieserite LASF55A	0.9722	Kieserite LASF55A	0.9282
HRL 43EC/2	Scolecite LAZE11	0.9013	Melanterite LASF44A	0.9677	Jarosite LASF27A	0.9252
HRL 43EC/2	Laumontite LAZE19	0.8858	Scolecite LAZE11	0.9614	Metavoltine LASF23A	0.9212
FRT AA7D	Romerite LASF48A	0.9051	Melanterite LASF44A	0.9439	Romerite LASF48A	0.9333
FRT AA7D	Voltaite LASF25A	0.8852	Romerite LASF48A	0.8994	Voltaite LASF25A	0.9060
FRT AA7D	Hexahydrate LASF56A	0.8651	Copiapite C1JB969	0.8988	Hexahydrate LASF56A	0.8941
FRT 863E	Melanterite LASF44A	0.9348	Melanterite LASF44A	0.9804	Romerite LASF48A	0.9392
FRT 863E	Metavoltine LASF23A	0.9151	Metavoltine LASF23A	0.9604	Amarantite LASF26A	0.9304
FRT 863E	Amarantite LASF26A	0.9001	Kieserite LASF55A	0.9596	Metavoltine LASF23A	0.9235
FRT 20BF9	Mg sulfate 799F366	0.8740	Mg sulfate 799F366	0.9349	Smectite BKR1JB173	0.8860
FRT 20BF9	Copiapite C1JB969	0.8617	Rozenite BKR1JB626B	0.9310	Mg sulfate 799F366	0.8848
FRT 20BF9	Botrygen LASF38A	0.8594	Copiapite C1JB969	0.9299	Copiapite BKR1LH052	0.8799

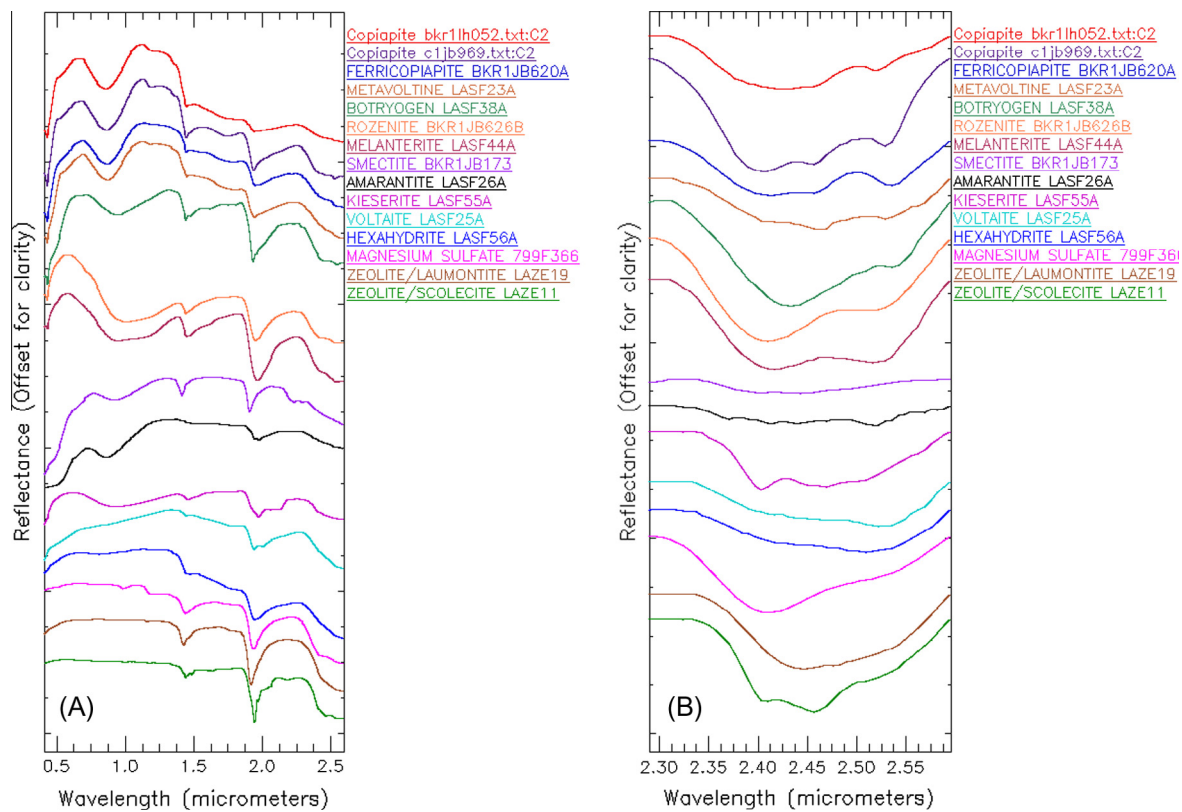


**Fig. 7.** (A) Spectra selected through spectral matching as candidate matches to the high SINDX ROI ratio spectra in the 2.29–2.6  $\mu\text{m}$  region. (B) Continuum-removed spectra from (a) over the 2.29–2.6  $\mu\text{m}$  range.

and of another sulfate mineral, or minerals, in several additional locations. Given the weak nature of the absorption features longwards of 2.3  $\mu\text{m}$  in the high SINDX ROI spectra, and the fact that these minerals occur as part of a mixture (as evidenced by the presence of a 2.2  $\mu\text{m}$  feature in association with these spectra that is not consistent with likely sulfate minerals), a robust identification of the actual phase, or phases, is difficult based solely on the “L” detector data.

The spectral matching metrics applied to the continuum-removed spectra over the 2.29–2.6  $\mu\text{m}$  range returned first, second, or third best matches to 17 library spectra (Table 3, Fig. 7). However, most of these spectra can be eliminated based on the presence or absence of spectral features at shorter wavelengths that are inconsistent with those of the high SINDX ROI ratio spectra. Of the 17 “match” spectra, three (romerite LASF48A, amarantite LASF26A, and the BKR1JB173 smectite) had absorption features

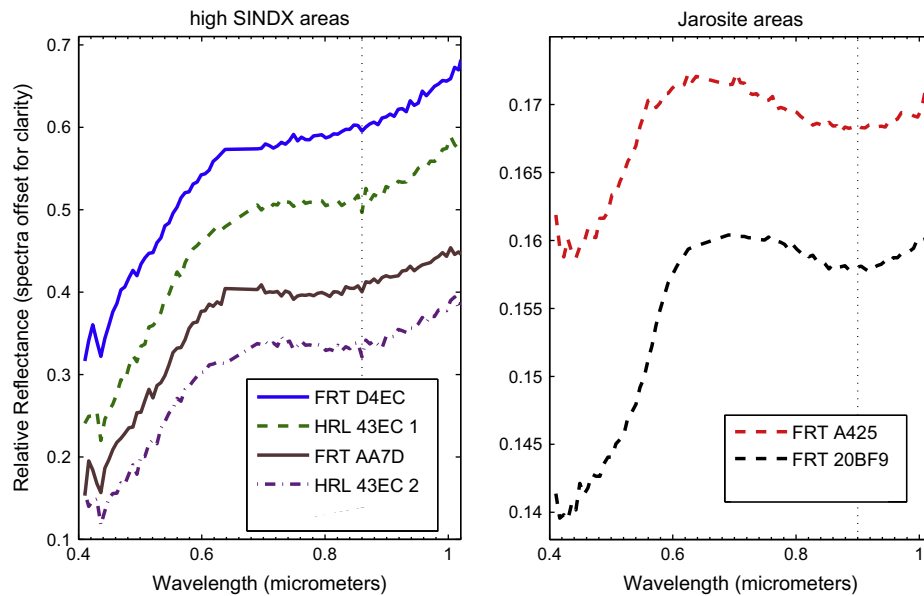


**Fig. 8.** (A) CRISM “S” spectrometer ratio spectra over high SINDX areas. Vertical dotted line indicates continuum-removed band center position of 0.86  $\mu\text{m}$ . Spectra offset for clarity. (B) “S” spectrometer ratio spectra over jarosite-bearing areas. Vertical dotted line indicates band center near 0.9  $\mu\text{m}$ . Note that while high SINDX areas examined here were generally higher in overall reflectance than the jarosite-bearing areas, the denominator spectra used and the offsetting of spectra for display indicate misleadingly high relative reflectance values for the high SINDX areas.

**Table 3**

Minerals identified from spectral matching metrics as potential matches to the high SINDX spectra in the 2.29–2.6 mm region with their chemical formulae and also a comment on whether they fit or had some mismatch in some other part of the CRISM spectral range with the high SINDX spectra.

Mineral	Formula	Library spectra	Match or mismatch with SINDX spectra at other wavelengths
Amarantite	$\text{Fe}^{3+}(\text{SO}_4)(\text{OH}) \cdot 3(\text{H}_2\text{O})$	LASF26A	Lacks triple absorption in 2.29–2.6 $\mu\text{m}$ range
Botryogen	$\text{MgFe}^{3+}(\text{SO}_4)_2(\text{OH}) \cdot 7(\text{H}_2\text{O})$	LASF38A	Poor match to NIR band
Copiapite	$\text{Fe}^{2+}\text{Fe}_3^{3+}(\text{SO}_4)_6(\text{OH})_2 \cdot 20(\text{H}_2\text{O})$	C1JB969, BKR1LH052	Good match
Ferricopiapite	$\text{Fe}_5^{3+}(\text{SO}_4)_6\text{O}(\text{OH}) \cdot 20(\text{H}_2\text{O})$	BKR1JB620A	Match in SWIR, lacks band near 1.15–1.18 $\mu\text{m}$
Hexahydrite	$\text{MgSO}_4 \cdot 6(\text{H}_2\text{O})$	LASF56A	No NIR band
Jarosite	$(\text{Na},\text{K})\text{Fe}_3^{3+}(\text{SO}_4)_2(\text{OH})_6$	LASF27A	SINDX spectra lack jarosite's 2.265 $\mu\text{m}$ band
Kieserite	$\text{MgSO}_4 \cdot \text{H}_2\text{O}$	LASF55A	No NIR band, SINDX spectra lack kieserite's 2.14 $\mu\text{m}$ band
Laumontite	$\text{CaAl}_2\text{Si}_4\text{O}_{12} \cdot 4(\text{H}_2\text{O})$	LAZE19	No NIR band
Melanterite	$\text{Fe}^{2+}\text{SO}_4 \cdot 7(\text{H}_2\text{O})$	LASF44A	Poor match in the VNIR
Metavoltine	$\text{Na}_6\text{K}_2\text{Fe}^{2+}\text{Fe}_3^{3+}(\text{SO}_4)_{12}\text{O}_2 \cdot 18(\text{H}_2\text{O})$	LASF23A	Good match in VNIR, lacks triple absorption in 2.29–2.6 $\mu\text{m}$ range
Mg sulfate	Unknown	799F366	No NIR band
Romerite	$\text{Fe}^{2+}\text{Fe}_3^{3+}(\text{SO}_4)_4 \cdot 14(\text{H}_2\text{O})$	LASF48A	Lacks triple absorption in 2.29–2.6 $\mu\text{m}$ range
Rozenite	$\text{Fe}^{2+}\text{SO}_4 \cdot 4(\text{H}_2\text{O})$	BKR1JB626B	Poor match in the VNIR
Scolecite	$\text{CaAl}_2\text{Si}_3\text{O}_{10} \cdot 4(\text{H}_2\text{O})$	LAZE11	No NIR band
Smectite	Unknown	BKR1JB173	Lacks triple absorption in 2.29–2.6 $\mu\text{m}$ range
Voltaite	$\text{K}_2\text{Fe}_5^{3+}\text{Fe}_3^{3+}\text{Al}(\text{SO}_4)_{12} \cdot 18(\text{H}_2\text{O})$	LASF25A	No NIR band

in the 2.29–2.6  $\mu\text{m}$  range that had band strengths that were only comparable to, weaker than, and/or poor visual matches to, those features in the CRISM high SINDX ratio spectra. As noted above, the high SINDX areas display a NIR band centered between 0.86 and 0.9  $\mu\text{m}$ , and another four of the library spectra identified by spectral matching (hexahydrite LASF56A, the Mg sulfate 799F366, laumontite LAZE19, and scolecite LAZE11) lack any NIR absorption band. The jarosite LASF27A has a 2.265  $\mu\text{m}$  band that is not observed in the high SINDX spectra and kieserite has a 2.14  $\mu\text{m}$  band that is not observed. Finally, melanterite and botryogen have VNIR absorptions that are dissimilar in terms of position and shape to the NIR band observed for the high SINDX areas. Out of the library spectra detected through the spectral matching, this leaves only the two copiapite spectra – C1JB969 and BKR1LH052, ferricopiapite BKR1JB620A, and metavoltine LASF26A as likely candidate matches for the high SINDX mineral phase.

The synthetic copiapite C1JB969 (Bishop et al., 2009) is an excellent match in the 2.29–2.6  $\mu\text{m}$  region to the high SINDX ROI ratio spectra. This is highlighted in Fig. 9 where this spectrum is

compared to the HRL000043EC high SINDX 1 region with dashed lines matching up the individual absorptions in this range.

Examination of the “S” detector data, and merged “S” and “L” detector data over the range of 0.4–1.3  $\mu\text{m}$  provides additional information that suggests that the phase causing the high SINDX values is copiapite. In this wavelength region, the high SINDX areas have near IR band minima ranging from approximately 0.86–0.9  $\mu\text{m}$ . These band minima are more consistent with a ferric iron sulfate such as jarosite or a mixed valence Fe-sulfate such as copiapite, or some ferric oxide or oxyhydroxide mineral than a ferrous iron sulfate.

As noted above, spectral features in the 2.29–2.6  $\mu\text{m}$  region are consistent with the high SINDX phase being copiapite. The NIR band of the high SINDX ROIs has a band minimum of 0.86–0.9  $\mu\text{m}$  – a shorter wavelength than the comparable feature of the jarosite occurrences in FRT0000A425 and FRT00020BF9 which have minima near 0.89 and 0.91  $\mu\text{m}$ . Also, the continuum-removed shape of that NIR band is different in laboratory spectra of copiapite and jarosite. In copiapite there is a definite long wavelength

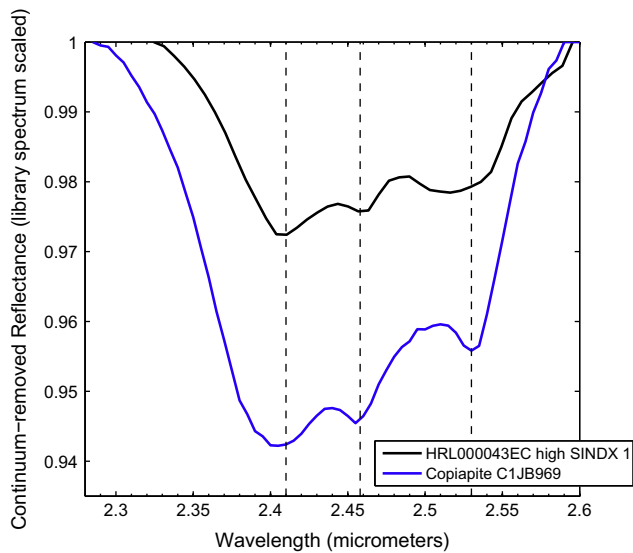


**Fig. 9.** Continuum-removed HRL000043EC high SINDX 1 ROI average ratio spectrum (black top) compared with synthetic copiapite C1JB969 spectrum (blue bottom) with vertical dashed lines highlighting individual absorptions. (For interpretation of the references to color in this figure legend, the reader is referred to the web version of this article.)

shoulder at approximately  $1.09\ \mu\text{m}$  with that shoulder manifesting more as a change in slope in jarosite spectra. In the  $0.4\text{--}1.3\ \mu\text{m}$  range spectra in Fig. 10b a continuum is superimposed on the spectra and that  $1.09\ \mu\text{m}$  shoulder is not as apparent, but still appears as a positive relief feature. As noted in Section 2, library spectra of copiapite have a weak ferrous iron band centered near  $1.17\ \mu\text{m}$ . The high SINDX ROI ratio spectra also generally display a weak band centered near  $1.15\ \mu\text{m}$  (Figs. 10b and 11a) which we attribute to being the copiapite ferrous iron band, although this feature is centered at a shorter wavelength than the known  $1.17\ \mu\text{m}$  ferrous iron band associated with copiapite (Fig. 11b). A number of the high SINDX areas also appear to have a sharp feature centered near  $0.43\ \mu\text{m}$  which is consistent with a  ${}^6\text{A}_{1g} \rightarrow ({}^4\text{A}_{1g}, {}^4\text{E}_g)$  band in library spectra of copiapite also centered at  $0.436\ \mu\text{m}$ . However, the lower signal-to-noise ratio at these short wavelengths makes a positive identification of this feature uncertain.

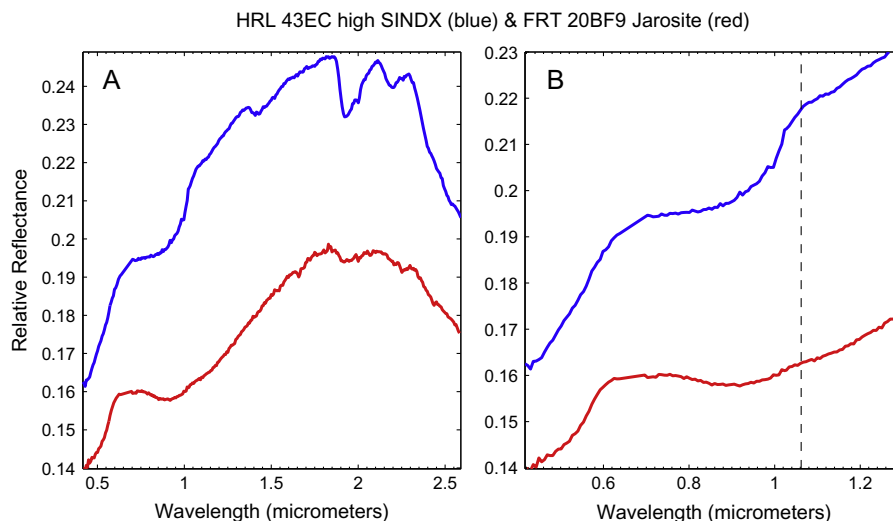


**Fig. 10.** (A) Merged full range spectra of high SINDX area in HRL000043EC and jarosite-bearing area in FRT00020BF9. (B) Spectra from (A) over the  $0.4\text{--}1.25\ \mu\text{m}$  range. Dashed line indicates positive relief spectral feature in high SINDX spectrum.

## 6.2. High spatial resolution imagery over high SINDX areas

Color HiRISE is not available over the high SINDX regions with the best examples of absorption bands in the  $2.29\text{--}2.6\ \mu\text{m}$  region; however, a weaker high SINDX area in the center of the HRL000043EC scene is covered by the HiRISE scene PSP\_005819\_2050 and a subsection of that scene is shown in Fig. 12. A buff color associated with polygonally fractured rock nominally represents the sulfate-bearing material. The polygonal fracturing resembles that previously described for the Al phyllosilicate unit (e.g., Michalski and Noe Dobrea, 2007), thus the sulfate-bearing material could be present as a coating or possibly as a vein fill (in a vein-rich matrix), like the calcium sulfates observed by the Opportunity rover in the bench unit and on the Matijevec Hill portion of Endeavour Crater (Squyres et al., 2012; Farrand et al., 2013a, 2013b).

## 6.3. Significance of mineral detections

Copiapite generally forms from the oxidation of pyrite although it can also form in association with volcanic fumaroles. With no evidence of volcanic activity in the Mawrth Vallis region, the more likely interpretation is that if copiapite is the phase responsible for the high SINDX response in the areas noted, then it did likely form from the weathering of pyrite. Copiapite and ferricopiapite can also precipitate from Fe- and S-rich waters such as those associated with AMD settings and can form as surface efflorescences in these AMD or acid sulfate soil situations (Bigham and Nordstrom, 2000; Jambor et al., 2000). Ferricopiapite was suggested as one of the primary ferric sulfates in S-rich soils examined by the Spirit rover in the Columbia Hills of Gusev crater (Johnson et al., 2007; Lane et al., 2008; Wang and Ling, 2011). Ferric sulfate formation from pyrite in low-temperature environments (similar to the temperature regime that is likely to have been extant on Mars at the time of the formation of the materials discussed here) has been studied in the Canadian arctic by West et al. (2009), Lacelle and Levéillé (2010), and Battler et al. (2013).

The presence of minerals such as copiapite or ferricopiapite at multiple locations across the northern Mawrth Vallis region suggests that there was some source of sulfur in these materials, possibly in the form of iron sulfides such as pyrite or pyrrhotite. The observations of other ferrous alteration phases throughout the Mawrth Vallis region (Bishop et al., 2008, in press) suggest that

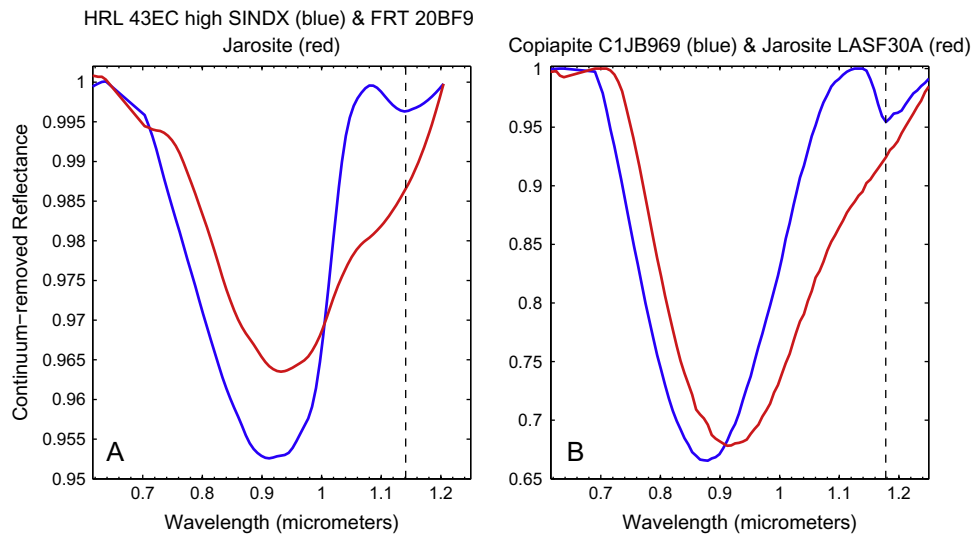


**Fig. 11.** (A) Continuum-removed CRISM high SINDX area spectrum and jarosite-bearing spectrum from HRL000043EC and FRT00020BF9. Spectra were smoothed with a Loess quadratic fit smoothing filter with a span of 0.16. Dashed line indicates band centered at 1.145  $\mu\text{m}$ . (B) Continuum-removed copiapite and jarosite library spectra with ferrous sulfate band centered at 1.175  $\mu\text{m}$  indicated by dashed line.

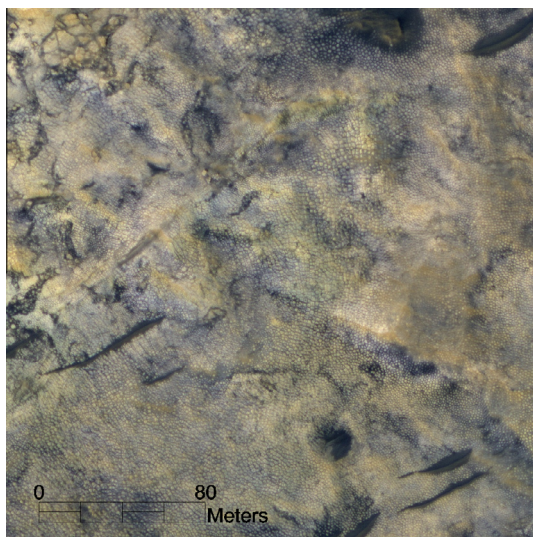


**Fig. 12.** Subsection of HiRISE color scene PSP\_005819\_2050 over high SINDX area mapped in CRISM scene HRL000043EC. Scene is centered at 24.5525°N, 33.9696°E and north is to the top. (For interpretation of the references to color in this figure legend, the reader is referred to the web version of this article.)

the presence of sulfides here is plausible. Generation of sulfates directly from sulfides has also been suggested by Fishbaugh et al. (2007) to explain the gypsum deposits in the northern Olympia Undae sand sea. A possible explanation for the origin of the sulfides would be from volcanic eruptions with high concentrations of sulfide minerals. SNC meteorites have more sulfides than comparable terrestrial igneous compositions (Lorand et al., 2005) and in many terrestrial volcanic rocks, sulfides (e.g., pyrrhotite or pyrite) can occur as accessory phases (Parat et al., 2011).

Weathering of sulfide minerals would have resulted in acidic conditions that could have contributed to acid leaching of materials to produce the observed ferric and mixed ferric/ferrous sulfates. The fact that the exposures of these minerals are restricted to patchy occurrences suggests either limited generation of these minerals or removal of wider exposures of these minerals subsequent to

formation, or both. One possible mode of formation of these types of Fe sulfates would involve the action of fluctuating ground water tables and locally acidic conditions due to sulfide exposure and oxidation, similar to processes that create terrestrial acid sulfate soils (Van Breeman, 1982; Wagner et al., 1982; Fanning et al., 1993). Such a scenario would also suggest that acidic alteration played a role in the formation of the upper Al phyllosilicate unit in Mawrth Vallis, as has recently been suggested by Horgan et al. (2013).

#### 6.4. Conclusions

The presence of spectral features consistent with the presence of ferric and mixed valence iron sulfates has been detected and studied in several CRISM scenes covering the northern portion of the Mawrth Vallis region of Mars. Initial evidence of these materials was in the form of high values of the SINDX and Doub2200 spectral parameters in these CRISM scenes. Closer examination of continuum-removed spectra over the high SINDX area indicated the presence of a 2.4 and 2.52  $\mu\text{m}$  doublet associated with the high SINDX areas in the volcano scan corrected and CIRRUS smoothed data. Division of ROI average spectra by those of spectrally flat regions in the same detector columns indicated that there was actually a triple absorption in the 2.29–2.6  $\mu\text{m}$  range.

To determine the identity of the phase responsible for the triple absorption band set, spectral matching metrics, including spectral feature fitting, a spectral similarity value, and a Pearsonian correlation coefficient, were applied to the 2.29–2.6  $\mu\text{m}$  range. Spectral matching with these metrics over this range identified 17 library spectra, but a process of elimination with regards to the presence or absence of a NIR absorption, the strength of the SWIR absorptions, and the fact that some of the spectral matches have features in the SWIR that were not observed in the high SINDX spectra, left only copiapite, ferricopiapite, and metavoltine as possible matches. Examination of information in the VNIR spectral region indicates that the high SINDX areas have a NIR absorption band with a minimum ranging from 0.86 to 0.9  $\mu\text{m}$ . While a number of Fe-bearing phases could cause such a feature, the presence of a weak band near 1.15  $\mu\text{m}$  and a sharp band near 0.43  $\mu\text{m}$  in a number of the high SINDX area ROIs is most consistent with copiapite.

Ferric and mixed valence iron sulfate minerals are associated with acid sulfate alteration such as occurs in terrestrial acid mine or acid rock drainage environments or in association with acid sulfate soils. We posit that the presence of these phases is evidence of acid sulfate alteration at the top of the Mawrth Vallis stratigraphic sequence. On Earth, the presence of minerals such as copiapite is associated with the weathering of pyrite or pyrrhotite. This might also be the case in this region with the iron sulfides coming either from underlying volcanic rocks in the region or along with volcanic ash from a sulfide-rich magma body, potentially coming from recently hypothesized calderas in nearby Arabia Terra (Michalski and Bleacher, 2013).

## Acknowledgments

Funding for initial work on this study was provided through the NASA Mars Data Analysis Program Grant Number NNX06AD87G. We thank two anonymous reviewers whose comments led to a substantially improved manuscript.

## References

- Abilio de Carvalho, O., Meneses, P.R., 2000. Spectral Correlation Mapper (SCM): An improvement on the Spectral Angle Mapper (SAM). In: Green, R.O. (Ed.), Proceedings of the Ninth JPL Airborne Earth Science Workshop. JPL Publication 00-18, pp. 65–74.
- Battler, M.M. et al., 2013. Characterization of the acidic cold seep emplaced jarosite Golden Deposit, NWT, Canada, as an analogue for jarosite deposition on Mars. *Icarus* 224, 383–398.
- Bibring, J.-P. et al., 2005. Mars surface diversity as revealed by the OMEGA/Mars Express observations. *Science* 307, 1576–1581. <http://dx.doi.org/10.1126/science.1108806>.
- Bibring, J.P. et al., 2006. Global mineralogical and aqueous Mars history derived from OMEGA/Mars Express data. *Science* 312, 400–404.
- Bigham, J.M., Nordstrom, D.K., 2000. Iron and aluminum hydroxysulfates from acid sulfate waters. In: Alpers, C.N., Jambor, J.L., Nordstrom, D.K. (Eds.), *Sulfate Minerals: Crystallography, Geochemistry, and Environmental Significance. Reviews in Mineralogy and Geochemistry*, vol. 40, pp. 351–403.
- Bishop, J.L., Murad, E., 2005. The visible and infrared spectral properties of jarosite and alunite. *Am. Miner.* 90, 1100–1107.
- Bishop, J.L. et al., 2008. Phyllosilicate diversity and past aqueous activity revealed at Mawrth Vallis, Mars. *Science* 321, 830–833. <http://dx.doi.org/10.1126/science.1159699>.
- Bishop, J.L., Dyar, M.D., Majzlan, J., Lane, M.D., 2009. Spectral properties of copiapites with variable cation compositions and implications for characterization of copiapite on Mars. *Lunar Planet. Sci.* 40, Abstract #2073.
- Bishop, J.L., Loizeau, D., Mckeown, N.K., Saper, L., et al., 2013. What the ancient phyllosilicates at Mawrth Vallis can tell us about possible habitability on early Mars. *Planet. Space Sci.*, in press. <http://dx.doi.org/10.1016/j.pss.2013.05.006>.
- Clark, R.N., Roush, T.L., 1984. Reflectance spectroscopy: Quantitative analysis techniques for remote sensing applications. *J. Geophys. Res.* 89, 6329–6340.
- Clark, R.N., Gallagher, A.J., Swayze, G.A., 1990. Material absorption band depth mapping of imaging spectrometer data using a complete band shape least-squares fit with library reference spectra. In: Green, R.O. (Ed.), Proceedings of the Second Airborne Visible/Infrared Imaging Spectrometer (AVIRIS) Workshop. JPL Publication 90-54, pp. 176–186.
- Clark, R.N. et al., 2007. USGS digital spectral library splib06a. U.S. Geological Survey, Digital Data Series 231.
- Cloutis, E.A. et al., 2006. Detection and discrimination of sulfate minerals using reflectance spectroscopy. *Icarus* 184, 121–157.
- Ehlmann, B.L. et al., 2011. Subsurface water and clay mineral formation during the early history of Mars. *Nature* 479, 53–60.
- Exelis Visual Information Systems, 2012. ENVI Classic Tutorial: Selected Hyperspectral Mapping Methods. ENVI 5.0 Manual.
- Fanning, D.S., Rabenhorst, M.C., Bigham, J.M., 1993. Colors of acid sulfate soils. In: Bigham, J.M., Ciolkosz, E.J. (Eds.), *Soil Color*. Soil Sci. Soc. Am. Spec. Publ. 31, pp. 91–108.
- Farrand, W.H., Glotch, T.D., Rice, J.W., Hurowitz, J.A., Swayze, G.A., 2009. Discovery of jarosite within the Mawrth Vallis region of Mars: Implications for the geologic history of the region. *Icarus* 204, 478–488.
- Farrand, W.H., Bell III, J.F., Johnson, J.R., Rice, M.S., Hurowitz, J.A., 2013a. VNIR multispectral observations of rocks at Cape York, Endeavour Crater, Mars by the Opportunity rover's Pancam. *Icarus* 225, 709–725.
- Farrand, W.H. et al., 2013b. Veins in Matijevic Hill lithologic units observed by Opportunity. *Lunar Planet. Sci.* 44, Abstract #2482.
- Fishbaugh, K.E., Poulet, F., Chevrier, V., Langevin, Y., Bibring, J.P., 2007. On the origin of gypsum in the Mars north polar region. *J. Geophys. Res.* 112, E07002. <http://dx.doi.org/10.1029/2006JE002862>.
- Flahaut, J., 2011. Minéralogie de Valles Marineris par imagerie hyperspectrale: Histoire magmatique et sédimentaire de la région. Doctoral Thesis, University of Lyon. 335pp.
- Gaudin, A., Dehouck, E., Mangold, N., 2011. Evidence for weathering on early Mars from a comparison with terrestrial weathering profiles. *Icarus* 216, 257–268.
- Gendrin, A. et al., 2005. Sulfates in martian layered terrains: The OMEGA/Mars Express view. *Science* 307, 1587–1591.
- Granahan, J., 2002. A compositional study of Asteroid 243 Ida and Dactyl from Galileo NIMS and SSI observations. *J. Geophys. Res.* 107 (E10), 5090. <http://dx.doi.org/10.1029/2001JE001759>.
- Horgan, B., Kahmann-Robinson, J.A., Bishop, J.L., Christensen, P.R., 2013. Climate change and a sequence of habitable ancient surface environments preserved in pedogenically altered sediments at Mawrth Vallis, Mars. *Lunar Planet. Sci.* 44, Abstract #3509.
- Jambor, J.L., Nordstrom, D.K., Alpers, C.N., 2000. Metal-sulfate salts form sulfide metal oxidation. *Rev. Mineral. Geochem.* 40, 303–350.
- Johnson, J.R. et al., 2007. Mineralogical constraints on sulfur-rich soils from Pancam spectra at Gusev crater, Mars. *Geophys. Res. Lett.* 34, L13202. <http://dx.doi.org/10.1029/2007GL029894>.
- Klingelhöfer, G. et al., 2004. Jarosite and hematite at Meridiani Planum from Opportunity's Mössbauer spectrometer. *Science* 306, 1740–1745.
- Lacelle, D., Levéillé, R., 2010. Acid drainage generation and associated Ca–Fe–SO<sub>4</sub> minerals in a periglacial environment, Eagle Plains, Northern Yukon, Canada: A potential analogue for low-temperature sulfate formation on Mars. *Planet. Space Sci.* 58, 509–521.
- Lane, M.D., Bishop, J.L., Dyar, M.D., King, P.L., Parente, M., Hyde, B.C., 2008. *Am. Mineral.* 93, 728–739.
- Langevin, Y., Poulet, F., Bibring, J.-P., Schmitt, B., Doute, S., Gondet, B., 2005. Sulfates in the north polar region of Mars detected by OMEGA/Mars Express. *Science* 307, 1584–1586.
- Le Deit, L. et al., 2012. Extensive surface pedogenic alteration of the martian Noachian crust suggested by plateau phyllosilicates around Valles Marineris. *J. Geophys. Res.* 117, E00J05. <http://dx.doi.org/10.1029/2011JE003983>.
- Loizeau, D., Mangold, N., Poulet, F., Ansan, V., Bibring, J.-P., Gondet, B., Langevin, Y., Masson, P., Neukum, G., 2010. Stratigraphy in the Mawrth Vallis region through OMEGA, HRSC color imagery and DTM. *Icarus* 205, 396–418.
- Lorand, J.P., Chevrier, V., Sautter, V., 2005. Sulfide mineralogy and redox conditions in some shergottites. *Meteorit. Planet. Sci.* 40, 1257–1272.
- McLennan, S.M. et al., 2005. Provenance and diagenesis of the Burns Formation, Meridiani Planum, Mars. *Earth Planet. Sci. Lett.* 240, 95–121.
- Michalski, J.R., Bleacher, J.E., 2013. Supervolcanoes within an ancient volcanic province in Arabia Terra, Mars. *Nature* 502, 47–52. <http://dx.doi.org/10.1038/nature12482>.
- Michalski, J.R., Noe Dobrea, E.Z., 2007. Evidence for a sedimentary origin of clay minerals in the Mawrth Vallis region, Mars. *Geology* 35 (10), 951–954. <http://dx.doi.org/10.1130/G23854A.1>.
- Michalski, J.R., Niles, P.B., Cuadros, J., Baldrige, A.M., 2013. Multiple working hypotheses for the formation of compositional stratigraphy on Mars: Insights from the Mawrth Vallis region. *Icarus* 226, 816–840.
- Murchie, S. et al., 2007. Compact Reconnaissance Imaging Spectrometer for Mars (CRISM) on Mars Reconnaissance Orbiter (MRO). *J. Geophys. Res.* 112, E05503. <http://dx.doi.org/10.1029/2006JE002682>.
- Murchie, S.L. et al., 2009. A synthesis of martian aqueous mineralogy after 1 Mars year of observations from the Mars Reconnaissance Orbiter. *J. Geophys. Res.* 114, E00D06. <http://dx.doi.org/10.1029/2009JE003342>.
- Noe Dobrea, E.Z. et al., 2010. Mineralogy and stratigraphy of phyllosilicate-bearing and dark mantling units in the greater Mawrth Vallis/west Arabia Terra area: Constraints on geological origin. *J. Geophys. Res.* 115, E00D19. <http://dx.doi.org/10.1029/2009JE003351>.
- Noe Dobrea, E.Z., Michalski, J.R., Swayze, G.A., 2011. Aqueous mineralogy and stratigraphy at and around the proposed Mawrth Vallis MSL Landing Site: New insights into the aqueous history of the region. *Mars* 6, 32–46. <http://dx.doi.org/10.1555/mars.2011.0003>.
- Parat, F., Holtz, F., Streck, M.J., 2011. Sulfur-bearing magmatic accessory minerals. *Rev. Mineral. Geochem.* 73, 285–314.
- Parente, M., 2008. A new approach to denoising CRISM images. *Lunar Planet. Sci.* XXXIX, Abstract #2528.
- Pelkey, S.M. et al., 2007. CRISM multispectral summary products: Parameterizing mineral diversity on mars from reflectance. *J. Geophys. Res.* 112, E08S14. <http://dx.doi.org/10.1029/2006JE002831>.
- Pieters, C.M., Hiroi, T., 2004. RELAB (Reflectance Experiment Laboratory) A NASA multiuser spectroscopy facility. *Lunar Planet. Sci.* XXXV, Abstract #1720.
- Roach, L.H., Mustard, J.F., Swayze, G., Milliken, R.E., Bishop, J.L., Murchie, S.L., Lichtenberg, K., 2010. Hydrated mineral stratigraphy of Ius Chasma, Valles Marineris. *Icarus* 206, 253–268.
- Squyres, S.W. et al., 2004. In situ evidence for an ancient aqueous environment at Meridiani Planum, Mars. *Science* 306, 1709–1714.
- Squyres, S.W. et al., 2012. Ancient impact and aqueous processes at Endeavour Crater, Mars. *Science* 336, 570. <http://dx.doi.org/10.1126/science.1220476>.
- Tosca, N.J., McLennan, S.M., Lindsley, D.H., Schoonen, M.A.A., 2004. Acid-sulfate weathering of synthetic martian basalt: The acid fog model revisited. *J. Geophys. Res.* 109, E05003. <http://dx.doi.org/10.1029/2003JE002218>.
- Van Breeman, N., 1982. Genesis, morphology, and classification of acid sulfate soils in coastal plains. In: Kittrick, J.A., Fanning, D.S., Hossner, L.R. (Eds.), *Acid Sulfate Weathering*. SSSA Special Pub. 10, pp. 95–108.

- Wagner, D.P., Fanning, D.S., Foss, J.E., Patterson, M.S., Snow, P.A., 1982. Morphological and mineralogical features related to sulfide oxidation under natural and disturbed land surfaces in Maryland. In: Kittrick, J.A., Fanning, D.S., Hossner, L.R. (Eds.), *Acid Sulfate Weathering*. Soil Sci. Soc. Am. Spec. Pub. 10, pp. 109–125.
- Wang, A., Ling, Z.C., 2011. Ferric sulfates on Mars: A combined mission data analysis of salty soils at Gusev crater and laboratory experimental investigations. *J. Geophys. Res.* 116, E00F17. <http://dx.doi.org/10.1029/2010JE003665>.
- West, L., McGown, D.J., Onstott, T.C., Morris, R.V., Suchecki, P., Pratt, L.M., 2009. High Lake gossan deposit: An Arctic analogue for ancient martian surficial processes. *Planet. Space Sci.* 57, 1302–1311.
- Woolridge, J.M., 2012. *Introductory Econometrics: A Modern Approach*, fifth ed. Cengage Learning, pp. 912.
- Wray, J.J., Squyres, S.W., Roach, L.H., Bishop, J.L., Mustard, J.F., Noe Dobra, E.Z., 2010. Identification of the Ca-sulfate bassanite in Mawrth Vallis, Mars. *Icarus* 209, 416–421.